PHYSICAL REVIEW B VOLUME 45, NUMBER 7 15 FEBRUARY 1992-I

Gallium vacancies and gallium antisites as acceptors in electron-irradiated semi-insulating GaAs

C. Corbel and F. Pierre
Centre d'Etudes Nucléaires de Saclay, Institut National des Sciences et Techniques Nucléaires, 91191 Gif-sur-Yvette CEDEX, France

K. Saarinen and P. Hautojärvi
Laboratory of Physics, Helsinki University of Technology, 02150 Espoo, Finland

P. Moser
Centre d'Etudes Nucléaires de Grenoble, Département de Recherche Fondamentale, 38041 Grenoble CEDEX, France
(Received 29 January 1991; revised manuscript received 10 June 1991)

Positron-lifetime measurements show that acceptors are produced in semi-insulating GaAs by 1.5-MeV electron irradiation at 20 K. Two types of acceptors can be separated. The first ones are negative vacancy-type defects which anneal out over a very broad range of temperature between 77 and 500 K. The second ones are negative ion-type defects which are stable still at 450 K. The data show that these two types of defects are independent and do not form close pairs. We attribute both to gallium-related defects. We identify the ion-type acceptors as isolated gallium antisites. The vacancy-type acceptors are identified as gallium vacancies which are isolated or involved in negatively charged complexes. The introduction rate of the gallium antisite is estimated to be 1.8 ± 0.3 cm^{-1} in the fluence range 10^{17}–10^{18} cm^{-2} for 1.5-MeV electron irradiation at 20 K.

I. INTRODUCTION

Most of the information on electron-irradiation-induced defects in GaAs has been obtained by electrical characterization or electron paramagnetic resonance (EPR) techniques. There is, however, increasing evidence that a large part of the irradiation-induced defects created by electron irradiation are not detected by deep-level transient spectroscopy (DLTS) experiments.[1–4] In addition, irradiation-induced defects may escape detection by EPR techniques when they are not in a paramagnetic state, even after photoexcitation (see, e.g., Refs. 5 and 6). The apparent dissymmetry in the production of defects by electron irradiation illustrates these difficulties. The arsenic antisite As_{Ga} and the arsenic vacancy V_{As}, both related to the displacements of As atoms, are identified by EPR measurements after irradiation. The EPR spectrum of the arsenic antisite As_{Ga}, first identified in as-grown GaAs,[7] has been found by several authors after electron[8,9] or neutron[10,11] irradiation (for reviews see Refs. 6 and 12). The EPR spectra due to the arsenic vacancy V_{As} has also been detected after electron irradiation.[5] However, the gallium vacancies and gallium antisites seem to escape detection. Their productions as stable defects are rarely mentioned[1–4,13] and quantitative data on their production rates are still lacking.

There is evidently a need to characterize irradiation-induced defects by additional techniques. Positron-lifetime spectroscopy is a suitable tool which has not yet been fully exploited. Its sensitivity to vacancy-type defects has been well demonstrated in semiconductors.[14–17] The positron lifetime in electron irradiated semi-insulating (SI) GaAs exhibits a strong temperature dependence which has been suggested to be due to positron trapping at gallium antisites.[18–20] To understand better the origin of this temperature dependence, we examine in this paper systematically the change of the positron lifetime as a function of temperature after various irradiation fluences.

The results of our study show that in SI GaAs after electron irradiation there are two types of negatively charged positron traps. One is dominant at high temperature, and we relate it to a negative monovacancy. The other is effective at low temperature, and we relate it to a negative ion. We associate these acceptors to gallium defects because arsenic defects are believed to be of donor type in SI GaAs.[5,13,17,21–25] The ions anneal at a temperature above 450 K, and they are produced with an introduction rate of 1.8 ± 0.3 cm^{-1}. We identify them as Ga_{As} antisites. The vacancies are identified as Ga vacancies, and they anneal between 77 and 500 K. They show a sharp partial annealing stage in the range 270–370 K.

The paper is divided into seven parts. The experiments are described in Sec. II. The temperature dependence of the positron lifetime is investigated as functions of fluence and annealing temperature in Sec. III. Section IV shows that positrons are trapped by vacancies and negative ions. Section V deals with the determination of the introduction rates of the negative ions as well as with the annealing properties of the vacancies and ions. The natures of the vacancies and negative ions are discussed in Sec. VI. The conclusions are given in Sec. VII.

II. EXPERIMENTAL DETAILS

Electron irradiations were performed at fluences from 10^{17} to 4×10^{18} cm^{-2} in undoped SI GaAs crystals pro-

vided by Thomson CSF. After such irradiations the crystals remain semi-insulating.[5,19] The 1.5- and 3-MeV electron irradiations were performed at 20 K with Van der Graaf accelerators at the Laboratoire des Solides Irradiés (Ecole Polytechnique-Paris) and Centre d'Etudes Nucléaires-Grenoble, respectively. After low-temperature irradiations, the samples were mounted at 77 or 100 K in a liquid N_2 cryostat for lifetime experiments. The isochronal annealings [30 min/(20–50 K)] were performed between 77 and 450 K. Some samples were also left to age at 300 K after annealings from 77 to 300 K for several weeks and then later mounted at 300 K in a lifetime spectrometer allowing higher counting efficiency.

Between the isochronal annealings, positron lifetimes were measured as a function of measurement temperature from 77 to 340 K. The measurements were performed in Saclay, Helsinki, and Grenoble with three different lifetime spectrometers with resolutions of 230–280 ps of full width at half maximum. The lifetime spectrometers were conventional[26,27] and the experimental details were the same as earlier.[15] The number of counts per spectrum was typically $(1-2)\times10^6$. After source corrections, one or two exponential decay components were used in the positron-lifetime spectra $n(t)$ to fit the experimental data

$$n(t)/n_0=I_1\exp(-t/\tau_1)+I_2\exp(-t/\tau_2)\ , \quad (1)$$

where n_0 is the total number of counts and I_i is the relative intensity of the lifetime τ_i. The average positron lifetime τ was calculated from the decomposition of the lifetime spectra as

$$\tau=I_1\tau_1+I_2\tau_2\ . \quad (2)$$

The center of mass of the experimental lifetime distribution was also calculated. In the numerical fittings, the expression (2) and the center of mass coincided within 2 ps.

The average positron lifetime is always accurately determined in spite of the uncertainties in the decomposition of the spectra. We shall see that many of the results in Sec. III concern the variation of this parameter because the decomposition of the spectra into several components is difficult in GaAs after electron irradiation especially at low temperature. For measurement temperatures ≥ 300 K the spectra can be reliably decomposed when sufficient number of counts are collected. Such spectra could be recorded only for aged samples.

It has been shown earlier in as-grown GaAs (Ref. 15) that the difference between τ_1 and τ_2 becomes too small (ratio $\tau_2/\tau_1<1.2$) at low temperature for reliable decomposition. This is due to positron trapping at negative ions. The decomposition is even more difficult in irradiated GaAs samples, because the irradiation itself produces more negative ions as it will be discussed below in this paper.

III. POSITRON-LIFETIME RESULTS

Before irradiation, the lifetime spectra in SI GaAs measured between 77 and 300 K are resolved into a single component. Its value is 230±1 ps and it shows only a small (0.5 ps over 100 K) temperature dependence due to lattice expansion.

After irradiation, the lifetime spectra in the various GaAs crystals are resolved into one or two components. The longest single lifetime component measured at 77 K is 263±2 ps. The spectra measured at room temperature after aging at 300 K can be decomposed into two components when the fluence increases from 0.1 to 7.6×10^{18} cm^{-2}. As shown in Table I, the long lifetime component τ_2 is 260±3 ps and the intensity of this long component increases from 61% to 87% with the fluence.

The positron-lifetime recovery as a function of annealing temperature is strongly dependent on the temperature at which the lifetime measurement is performed. This property is observed for various fluences after 3-MeV as well as after 1.5-MeV irradiations. After annealings in the range 500–600 K, the lifetime shows no recovery at any measurement temperature. The absence of a recovery stage in the range 500–650 K is a characteristic independent of the irradiation energy and fluence.

The positron-lifetime recovery is illustrated in Fig. 1 after 3 MeV irradiation at the fluence 4×10^{18} cm^{-2}. In this figure, the average lifetime is shown as a function of annealing temperature for the three measurement temperatures of 100, 250, and 341 K. For a given measurement temperature, the annealing curve starts after annealing of the sample above the measurement temperature. Three types of recovery curves are obtained when the measurement temperature after each annealing is varied from 77 to 341 K. The curve 100 K (250 and 341 K, respectively) in Fig. 1 represents the annealing curves obtained when the measurement temperature is fixed in the range 77–150 K (200–300 K and 310–350 K, respectively). Figure 1 shows that the recovery is more com-

TABLE I. Decompositions of the lifetime spectra at 300 K after 1.5-MeV electron irradiation at 20 K and after aging several weeks at room temperature. The decomposition is also shown after annealing at 425 K for the crystals irradiated at 1.3×10^{18} cm^{-2}. The value τ_b in the table is calculated in the framework of the one-defect trapping model as $\tau_b^{-1}=I_1/\tau_1+I_2/\tau_2$ (see Sec. IV in the text). The asterisk denotes aging.

Fluence (10^{17} cm^{-2})	T_A (K)	τ (ps)	τ_1 (ps)	τ_2 (ps)	I_2 (%)	τ_b (ps)
1	300*	234±1	195±14	259±10	60±10	229
5	300*	240±1	180±10	264±7	70±8	232
13	300*	243±1	163±17	259±3	84±5	237
13	425	241±1	160±17	255±3	85±5	234
76	300*	249±1	176±21	261±3	87±6	246

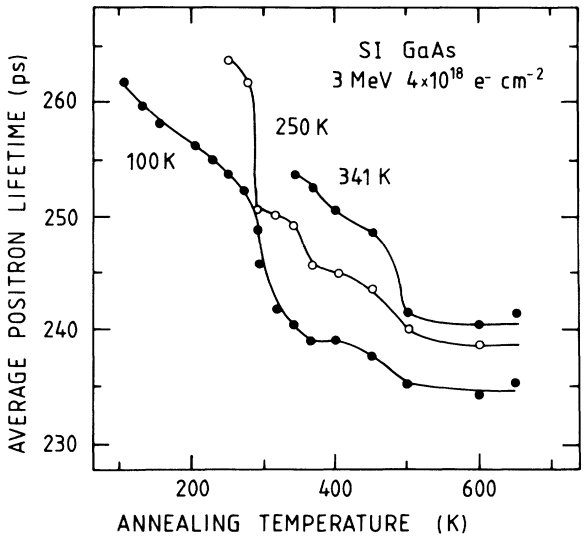

FIG. 1. Recovery of the positron lifetime in semi-insulating GaAs after 3-MeV electron irradiation at 20 K at the fluence 4×10^{18} cm^{-2}. Influence of the measurement temperature.

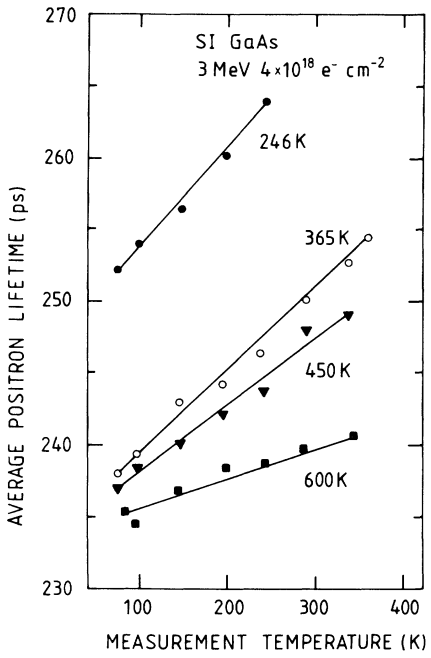

FIG. 2. Temperature dependence of the positron lifetime in semi-insulating GaAs after 3-MeV electron irradiation at 20 K at the fluence 4×10^{18} cm^{-2}. The annealing temperature is indicated for each curve and the annealing time is 30 min.

plete at a low measurement temperature than at a high measurement temperature. After the 650-K annealing, the average positron lifetime is 241±1 ps when measured at 341 K and only 235±1 ps when measured at 100 K. Figure 1 shows that the recovery stages are affected by the measurement temperature. At low temperatures (see the curve 100 K in Fig. 1), three stages can be defined. Below 270 K, a smooth recovery stage takes place where the lifetime decreases about 33%. It is followed by a sharp stage between 270 and 370 K where the amount of recovery is about 50%. Then a small recovery corresponding to 13% occurs between 400 and 500 K. As the measurement temperature increases, these stages become more or less visible and deformed. At intermediate measurement temperatures (see the 250 K curve in Fig. 1), the smooth stage below 270 K disappears progressively, the stage between 270 and 370 K exhibits a very steep step around room temperature, and the 400–500 K stage becomes more pronounced. At high measurement temperatures (see the curve 341 K in Fig. 1), the 400–500 K stage is still further amplified: its height increases from 13% to 30%. As mentioned above, at any measurement temperature, no recovery is observed in the temperature range 500–650 K.

The recovery in Fig. 1 after electron irradiation varies with the measurement temperature because the positron average lifetime is strongly temperature dependent. The temperature dependence is shown in Figs. 2–4 for various fluences and electron energies.

It can be seen in Fig. 2 that the positron lifetime increases linearly between 77 and 350 K in the crystals irradiated with 3 MeV electrons at the fluence 4×10^{18} cm^{-2}. The slope is nearly independent of the annealing temperature up to 365 K, whereafter it decreases as the annealing temperature increases up to 650 K.

In the crystals irradiated with 1.5 MeV electrons at 5×10^{17} cm^{-2}, the temperature dependence is not any more linear after annealing and aging at 300 K as seen in Fig. 3. The lifetime increases between two plateaus which tend to be formed at low and high temperatures. This behavior is also observed in Fig. 4 for the crystals irradiated at 1×10^{17} cm^{-2}. The tendency to form plateaus appears over a wide range of annealing temperatures, from 175 to 300 K. It is worth noting that the tempera-

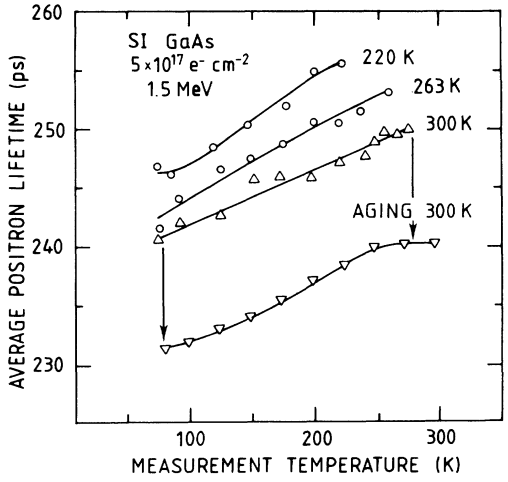

FIG. 3. Temperature dependence of the positron lifetime in semi-insulating GaAs after 1.5-MeV electron irradiation at 20 K at the fluence 5×10^{17} cm^{-2}. The annealing temperature is indicated for each curve and the annealing time is 30 min. Measurements after aging at 300 K are indicated by the vertical arrows.

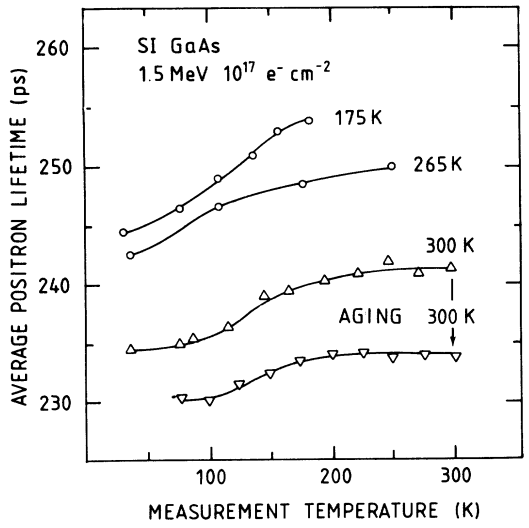

FIG. 4. Temperature dependence of the positron lifetime in semi-insulating GaAs after 1.5-MeV electron irradiation at 20 K at the fluence 10^{17} cm^{-2}. The annealing temperature is indicated for each curve and the annealing time is 30 min. Measurements after aging at 300 K are indicated by the vertical arrows.

tures below and above which the plateaus start are independent of the value of the lifetimes on the plateaus. In Fig. 4 the curve measured after aging at 300 K is below the curve measured after 30 min annealing at 300 K. However, the plateau at low temperature starts below 100 K and the plateau at high temperature starts around 200 K for both curves.

Figure 5 shows how the fluence for 1.5-MeV electron irradiation affects the temperatures at which the plateaus in the curve $\tau = f(T)$ are formed. As fluence increases by an order of magnitude from 10^{17} to 1.3×10^{18} cm^{-2} the temperature where the low-temperature plateau ends remains 100 K. Contrary, as fluence increases by a factor 10, the temperature where the high-temperature plateau starts shifts from 200 to 350 K. It is important to notice that in spite of this big temperature shift, there are very small changes in the lifetime values on the plateaus: τ varies by 3 ps only.

After electron irradiation, the decomposition of the lifetime spectra into two components is more difficult at low temperature than at high temperature. This is illustrated in Fig. 6 for the spectra measured in the crystals after 1.5-MeV irradiation at the fluences of 10^{17} and 5×10^{17} cm^{-2} and aging at 300 K. The lifetime spectra at 300 K can be resolved into two components and the longest component τ_2 has the value 260±3 ps (see also Table I). For the spectra measured at lower temperature, there is still a long component close to 260 ps but the decomposition is rather difficult. In Fig. 6, the long lifetime in the spectra has been fixed to 260 ps to reduce the statistical scattering of the decomposition. The intensity I_2 of the lifetime of 260 ps decreases with decreasing temperature.

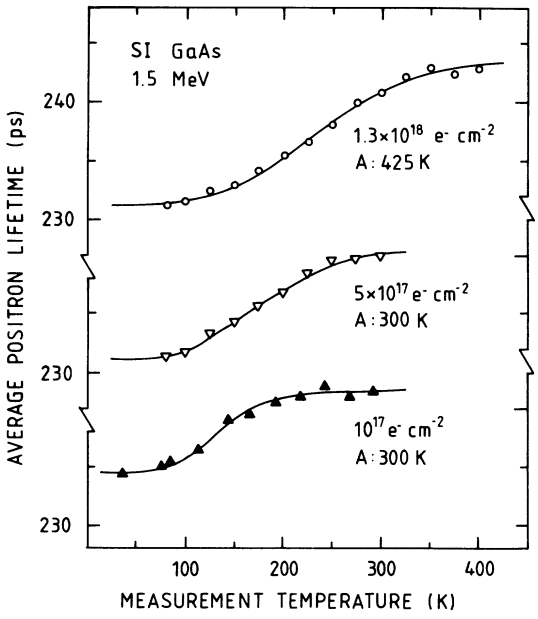

FIG. 5. Fluence effects on the temperature dependence of the positron lifetime in semi-insulating GaAs after 1.5-MeV electron irradiation at 20 K. For the fluences 1×10^{17} and 13×10^{17} cm^{-2} the measurements were performed after 30-min annealing at 300 and 425 K, respectively. For the fluence 5×10^{17} cm^{-2} the measurements were performed after aging at 300 K. The solid lines are based on the fits to Eq. (5).

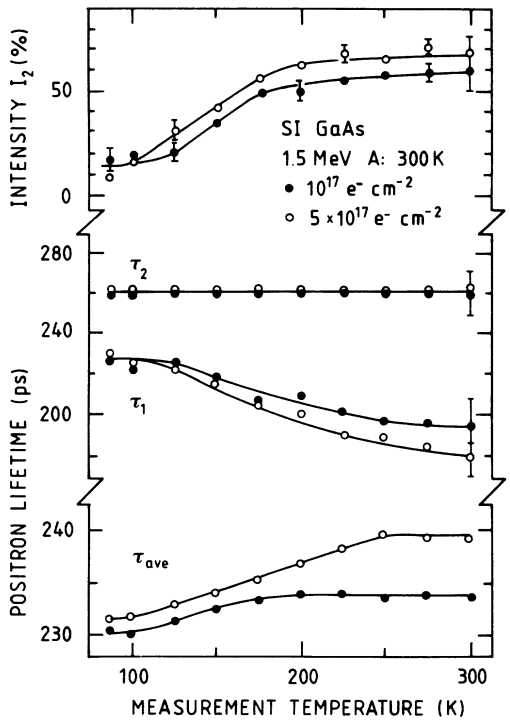

FIG. 6. Decomposition of the positron-lifetime spectra as a function of temperature in semi-insulating GaAs after 1.5-MeV electron irradiation at 20 K. The fluences are 10^{17} and 5×10^{17} cm^{-2} and the aging temperature is 300 K. The lifetime τ_2 has been fixed to 260 ps in the decompositions, except in the analysis of the data measured at 300 K.

The shorter lifetime τ_1 gets roughly a value of 230 ps at low temperatures of 77–125 K.

IV. VACANCIES AND NEGATIVE IONS AFTER ELECTRON IRRADIATION

In this section, we explain the temperature dependence of the positron lifetime after electron irradiation in SI GaAs in terms of competition of the positron trapping between vacancies and negative ions.

The lifetime of 230±1 ps measured in SI GaAs before irradiation agrees well with previous measurements[15] and it has been attributed to positron annihilation from the delocalized state in the bulk.

Electron irradiations at 1.5 and 3 MeV energies induce positron trapping at vacancy-type defects in SI GaAs. In Figs. 1–4, the increase of the average positron lifetime above 230 ps gives clear evidence of this positron trapping. It is well established[26,27] that vacancy-type defects form deep potential wells for positrons where positrons are trapped with binding energies of about 0.5–2 eV. Positrons trapped at vacancy-type defects annihilate with lifetimes longer than in bulk, because in the regions of the vacancy-type defects positrons encounter electron densities lower than in the perfect lattice. The decomposition of the lifetime spectra in 1.5-MeV irradiated SI GaAs shows that the lifetime due to the vacancy-type defects is 260±3 ps before and after annealing at 300 K. After 3-MeV irradiation, the positron-lifetime spectrum is one-componential with $\tau=263\pm3$ ps both at the measurement temperature of 100 K after 100-K annealing and at the measurement temperature of 250 K after 250-K annealing (Fig. 1). This behavior suggests that the lifetime value $\tau=263\pm3$ ps corresponds to positron trapping saturation, where all positrons annihilate at vacancy defects. The positron lifetime at vacancy defects is thus constant at a value of about 260±3 ps at all temperatures studied in this work. Similar results have been obtained earlier after 3- (Ref. 2) and 1.5-MeV (Refs. 18 and 19) electron irradiations. The lifetime of 260 ps in GaAs is a typical value which, according to positron-lifetime calculations,[28,29] can be expected for positrons trapped at monovacancies. According to these calculations,[28,29] divacancies V_{As}-V_{Ga} would produce a significantly higher lifetime of 310–320 ps. Thus we conclude that positrons annihilating with the lifetime of 260 ps are trapped at monovacancy defects. There is no way from the lifetime itself to conclude whether the monovacancy is isolated or involved in a defect complex.

In irradiated SI GaAs, the lifetime recovery exhibits characteristics strongly dependent on the temperature at which it is investigated. This property has been found earlier,[18,19] but we study it here in a more systematic way. By examining the variation of the positron lifetime as a function of temperature after various irradiations, we shall be able to properly discuss the origin of this strong temperature dependence.

The increase of the positron lifetime with measurement temperature in Figs. 2–5 means that the annihilation at the monovacancies has a higher probability at higher temperature. The temperature range where the probability increases varies with the irradiation and annealing conditions. We focus on Fig. 5 which clearly shows fluence effects after 1.5-MeV irradiation. As the influence increases by an order of magnitude from 10^{17} to 1.3×10^{18} cm^{-2}, the temperature region where the probability increases between the low-temperature plateau and the high-temperature plateau becomes wider. Two points are important to notice. (i) The temperature below which the probability becomes independent of the temperature is rather insensitive to the fluence and is located around 100 K. (ii) The temperature above which the probability remains constant increases with fluence. The increase is big, from 200 to 350 K when the fluence increases by a factor of 10. In order to understand this temperature shift, we turn our attention to the properties of the positron trapping coefficient at the vacancies.

The positron trapping coefficient per monovacancy μ_v is related to the trapping rate at monovacancies κ_v by the relation (3)

$$\mu_v=\frac{\kappa_v}{c_v}\ , \tag{3}$$

where c_v is the monovacancy concentration. The trapping rate at vacancies κ_v can be calculated in the framework of the trapping model[26,27] from the curves $\tau=f(T)$ displayed in Fig. 5. In the high-temperature region of the curves, the decompositions of the lifetime spectra are consistent with the trapping model where only the vacancies act as trapping centers for positrons. This is shown in Table I for the curves corresponding to the fluences 5×10^{17} and 1.3×10^{18} cm^{-2}. The value τ_b calculated in the one-defect trapping model ($1/\tau_b=I_1/\tau_1+I_2/\tau_2$) agrees well with the lifetime of the delocalized positron. We can then calculate the trapping rate at vacancies κ_v in the framework of the trapping model using the relation

$$\kappa_v=\frac{1}{\tau_b}\frac{\tau-\tau_b}{\tau_v-\tau}\ , \tag{4}$$

where τ_b is the bulk lifetime (230 ps) and τ_v is the lifetime at a monovacancy defect (260 ps). The values of κ_v are given in Table II.

In the high-temperature region where τ is constant, the trapping rate κ_v is then constant according to Eq. (4).

TABLE II. Average lifetimes τ on the high-temperature plateaus of the curves in Fig. 5 and corresponding trapping rates at vacancies κ_v in the one-defect trapping model. The crystals irradiated at 20 K have then been isochronally annealed up to T_A or aged at T_A^*. The asterisk denotes aging.

Fluences (10^{17} cm^{-2})	T_A (K)	Average lifetime (ps)	Trapping rate κ_v (10^9 s^{-1})
1	300	241±1	2.5±0.6
5	300*	240±1	2.2±0.6
13	425	243±1	3.3±0.6

Equation (3) indicates that the positron trapping coefficient per monovacancy $\mu_v = \kappa_v / c_v$ is also constant in this high-temperature region. According to the curve $\tau = f(T)$ after the fluence 10^{17} cm^{-2} in Fig. 5, μ_v is independent of temperature above 200 K. For the fluences 5×10^{17} and 1.3×10^{18} cm^{-2}, μ_v becomes independent of temperature only above 250 and 350 K, respectively. These temperature shifts are striking. It is even more striking for the fluences 10^{17} and 5×10^{17} cm^{-2} as the values of κ_v on the high-temperature plateaus differ by less than 14% (see Table II). It is rather difficult to think of a positron trapping mechanism at vacancies which would lead to such a behavior of the positron trapping coefficient μ_v.

It is unlikely that this temperature dependence reflects an intrinsic property of the positron trapping coefficient at the monovacancies. On the other hand, it is easy to explain the shift of the temperature by assuming that positrons are thermally emitted from other defects than the vacancies when temperature increases. Consequently, we propose that a competition between positron trapping at vacancies and at other defects results in the temperature dependence of the annihilation probability at vacancies. Evidence of the existence of other defects than the vacancies is given by the decomposition of the lifetime spectra after the high fluence irradiations of 1.3×10^{18} and 7.6×10^{18} cm^{-2}. In these heavily irradiated crystals, the one-defect trapping model is not valid at room temperature after 300 K aging: Table I shows that the lifetime τ_b calculated in the one-defect trapping model is longer than the lifetime of the delocalized positrons. To determine the nature of those other defects, we examine the positron annihilation properties which can be deduced from Figs. 2–6.

The defects trapping the positron in competition with the vacancies become effective at low temperatures. These defects give rise to a lifetime well below 260 ps, since the positron lifetime decreases when temperature decreases. At low temperature the positron lifetimes in Figs. 3–6 tend towards a limit corresponding to 230 ps. This lifetime value is the same as that measured in the bulk. Positron trapping characterized by bulk lifetime points out to positron trapping at Rydberg states around negative ions, as it has been discussed earlier.[30] These negative ions are shallow traps for positrons in the sense that the positron binding energy is small ($\sim$50 meV). Positrons can easily escape from the shallow traps once they gain enough energy from the crystal temperature. It is this thermal detrapping (Ref. 30, and references therein) from negative ions we observed in Figs. 2–6. With increasing temperature, the ratio of the detrapping rate to the trapping rate increases and the probability of the annihilation at the negative ions decreases to the benefit of the annihilation at vacancies.

We will examine now whether the negative ions and the vacancies form close pairs (first or second neighbors) or act as separated entities. We assume first that the ions and vacancies form close pairs and examine whether the trapping properties of a close pair correspond to the positron trapping characteristics experimentally observed. For vacancy-ion pairs, the temperature dependence of the annihilation probability at the vacancy is still governed by the detrapping from the ions. As the vacancy and ion concentrations are equal when close pairs are formed, the temperature dependence of the average lifetime τ is completely determined by the trapping rate κ_v in the high-temperature plateau. The experimental situation we observe here is different: in Fig. 4, the temperature dependence is the same for different values of τ in the high-temperature plateaus. In Fig. 5, the temperature dependence varies strongly for nearly the same τ values in the high-temperature plateaus. This shows that the concentration of ions and vacancies is not the same. We can therefore conclude that the irradiated crystals contain vacancies and ions which are well separated defects. Supporting this conclusion, we shall see in Sec. V that the concentration of negative ions remains constant when the concentration of vacancies decreases.

For given trapping rates at vacancies and negative ions, the temperature dependence of τ is then controlled by the detrapping from the negative ions. In the following, we discuss qualitatively some characteristics of the temperature dependence displayed by τ in Figs. 4 and 5.

In Fig. 4, the τ value on the high-temperature plateau decreases from 241 to 234 ps after 300 K aging. This corresponds to a decrease of the trapping rate at vacancies from 2.2 to 0.6 ns^{-1}. However, both the low- and high-temperature plateaus of the lifetime occur at the same temperatures in the two cases, below 100 K and above 200 K. This leads to conclude that the temperatures where the plateaus end and start are independent on the vacancy trapping rate. It indicates here that the trapping rate at the ions and, consequently, the detrapping rate from the ions are the same before and after aging.

In Fig. 5, the trapping rate at the vacancies is nearly the same for the fluence 10^{17} and 5×10^{17} cm^{-2}, 2.5 and 2.2 ns^{-1}, respectively. However, there is a shift of 50 K between the temperatures at which the high-temperature plateaus start. As discussed above, the temperature shift is related more to the trapping rate at negative ions than vacancies. The trapping rate at the negative ions can be qualitatively compared by comparing the lifetime values of the low-temperature plateau. In Fig. 5, the lifetime below 100 K is lower for the curve 5×10^{17} cm^{-2}. This indicates that the positron trapping at the ions is higher after 5×10^{17} cm^{-2} than after 10^{17} cm^{-2} irradiation. It may thus be concluded that for a given concentration of vacancies, the high-temperature plateau region begins at higher temperatures when the positron trapping at ions increases. On the other hand, the temperature where the low-temperature plateau starts seems to be independent of the positron trapping rate at vacancies and ions. It is about 100 K for the three curves in Fig. 5 although the irradiation fluence varies by an order of magnitude.

In summary, the temperature dependence of the average positron lifetime after electron irradiation is due to the existence of two types of defects trapping positrons. The vacancy-type defects are deep traps whereas the negative ion-type defects are shallow traps. The probability that the positrons annihilate at the negative ions increases strongly at low temperature preventing the trapping by the vacancy-type defects.

V. INTRODUCTION RATE OF THE NEGATIVE IONS

In this section, we examine the properties of the positron trapping at the negative ions. The analysis of the experimental results shows that the negative ions are produced by irradiation. The ions are very stable and anneal above 450 K. The vacancies anneal over a wide temperature range from 77 to 500 K with a main stage centered around room temperature.

The general expression for τ when negative ions and vacancies both act as independent trapping centers can be easily calculated in the trapping model. The kinetic equations describing the positron transitions from the bulk state to the localized state at the ions or at the vacancies are solved for the stationary state (see the Appendix). The average positron lifetime can be written as

$$\tau=\tau_v\frac{(\lambda_v+\kappa_v)\left[\frac{\lambda_{st}}{\kappa_{st}}+\frac{\delta}{\kappa_{st}}\right]+\lambda_v}{(\lambda_b+\kappa_v)\left[\frac{\lambda_{st}}{\kappa_{st}}+\frac{\delta}{\kappa_{st}}\right]+\lambda_{st}}, \tag{5}$$

where $\lambda_b=1/\tau_b=4.35\ \text{ns}^{-1}$ is the annihilation rate in bulk, $\lambda_v=1/\tau_v=3.85\ \text{ns}^{-1}$ is the annihilation rate at the vacancy defects, κ_v is the trapping rate at the vacancy, λ_{st} is the annihilation rate at the negative ions, κ_{st} is the trapping rate at the negative ions, and δ is the thermal detrapping rate from the negative ions. The expression (5) shows that for a given ratio κ_v/κ_{st}, the average lifetime tends towards the average lifetime due to the vacancy defects when the detrapping rate from the negative ions increases. In analogy to the carrier capture and emission rates at a carrier trap, the positron trapping and detrapping rates at a positron trap are related at thermal equilibrium. A thermodynamic approach[31] gives that the positron trapping and detrapping rates are related by the expression

$$\frac{\delta}{\kappa_{st}}=\frac{1}{c_{st}}\left[\frac{m^*}{2\pi\hbar^2}\right]^{3/2}(k_bT)^{3/2}\exp\left[-\frac{E_b}{k_bT}\right], \tag{6}$$

where c_{st} is the concentration of positron traps, i.e., here the negative ions, and E_b the positron binding energy at them, i.e., its ionization energy to the bottom of its lowest band. The detrapping from a positron trap can be observed below room temperature when the ionization energy of the positron is low ($\sim$50 meV), i.e., the positron trap is shallow. In Eqs. (5) and (6), the quantities κ_{st} and c_{st} are related by

$$\kappa_{st}=\mu_{st}c_{st}, \tag{7}$$

where μ_{st} is the positron trapping coefficient per ion.

In the Appendix, we have numerically studied how the shape of the curve $\tau=f(T)$ evolves when only one parameter κ_v, κ_{st}, or E_b is changed in Eqs. (4) and (5). The results confirm the qualitative analysis made for the curves in Figs. 4 and 5. The evolution of the curves $\tau=f(T)$ (Fig. 10), when κ_v varies with the ratio κ_v/κ_{st} in the range 0.05–1, reproduces well the experimentally observed behavior in Figs. 3 or 4 when aging at 300 K reduces the trapping rate at vacancies. The shape of the curves obtained by varying the trapping rate at ions κ_{st} (Fig. 11) evolves in the same way as in Fig. 5. The evolution of the curves in Fig. 5 corresponds to an increase of the positron trapping rate at negative ions as fluence increases.

We can further analyze the fluence effects displayed in Fig. 5 as follows. For each curve $\tau=f(T)$, if the positron trapping rates at vacancies and negative ions are known, the binding energy E_b and the concentration of negative ions c_{st} can be determined by fitting Eq. (5) to the experimental lifetime data. Let us assume that the positron trapping rates at vacancies and negative ions are temperature independent. Then the positron trapping rates at vacancies and negative ions can be calculated from the lifetimes at the plateaus in Fig. 5. The trapping rate at the vacancies κ_v is calculated as explained above by using Eq. (4), which is valid when the detrapping from the negative ions is complete. The values κ_v in Table II have been estimated with the assumption that the detrapping rate from the ions was total on the high-temperature plateau. However, to obtain a calculated curve $\tau=f(T)$ which fits well to the experimental data in the region of the high-temperature plateau, the value of κ_v has to be increased slightly above that given in Table II. The adjusted values of κ_v are given in Table III. These values of κ_v are higher than those given in Table II because, due to the exponential dependence of the detrapping from the ions, the high-temperature plateaus observed in Fig. 5 correspond to lifetime values which are in fact still sensitive to the trapping at the ions. For the fluence 10^{17} cm^{-2}, there is less than 10% of difference for κ_v in Tables II and III because for this curve the trapping at ions is small, the detrapping being nearly complete at 200 K. The trapping rate at the negative ions is calculated using the expression

$$\kappa_{st}=\frac{\kappa_v(\tau_v-\tau)+\lambda_b(\tau_b-\tau)}{\tau-\tau_{st}}, \tag{8}$$

which is valid below 100 K where the positron detrapping δ can be neglected. Table III gives the values which have been used for the fitting of each curve in Fig. 5. The resulting values obtained for E_b and c_{st} are also shown in Table III. In the fitting procedure only the statistical deviations of the average lifetime have been considered.

TABLE III. Trapping rates at vacancies κ_v and negative ions κ_{st} after 1.5-MeV electron irradiation and the fitted values of the positron binding energy E_b at the ions and the ion concentration c_{st}. The crystals irradiated at 20 K have then been isochronally annealed up to T_A or aged at T_A^*. The asterisk denotes aging.

Fluence (10^{17} cm^{-2})	T_A (K)	κ_v (ns^{-1})	κ_{st} (ns^{-1})	E_b (meV)	c_{st} (10^{17} cm^{-3})
1	300	2.80	11.5	38±7	1.3±0.8
5	300*	2.90	59.4	37±4	10±3
13	425	4.97	115	45±3	24±4

The positron binding energy E_b for irradiation-induced negative ions in SI GaAs is then found to be 41±4 meV independent of the fluence. The concentration of ions c_{st} increases from 1.3×10^{17} to 2.4×10^{18} cm^{-3} as the fluence increases from 10^{17} to 1.3×10^{18} cm^{-3}.

The temperature dependence of the trapping coefficient at negative traps is expected to be $T^{-1/2}$ (Ref. 42). In Sec. VI, we shall see that the vacancies are also negatively charged. The results displayed in Table III are affected by less than 20% when a temperature dependence $T^{-1/2}$ is allowed for the trapping coefficient at the vacancies and ions. The explanation for this small effect is that in the temperature range where the dependence in $T^{-1/2}$ is important, the temperature dependence of τ in Eq. (5) is dominated by the exponential Boltzmann factor of δ.

Figure 7 gives the Arrhenius plot of the ratio of the detrapping and the trapping rates at the ions

$$\frac{\delta}{\kappa_{st}}=\frac{\lambda_v(\tau\lambda_{st}-1)}{\kappa_v-\lambda_v(\tau\lambda_b+\tau\kappa_b-1)}-\frac{\lambda_{st}}{\kappa_{st}} \tag{9}$$

calculated for each fluence using the experimental curve $\tau=f(T)$ in Fig. 5.

The solid lines in Fig. 7 are obtained by calculating the ratio δ/κ_{st} from Eq. (6) using the fitted values for E_b and c_{st} from Table III. The ratios δ/κ_{st} follow well the Arrhenius law over one decade and half. The slope is the same for the three fluences reflecting the same positron binding energy at the ions. The decrease of the ratio as fluences increases is due to the increase of the ion concentration.

In Fig. 8, it can be seen that the concentration of negative ions increases linearly with the irradiation fluence. The introduction rate is high, 1.8±0.3 cm^{-1}. It is important to stress that the points fits well to a straight line although the curves $\tau=f(T)$ for the different fluences in Fig. 5 have been measured after different annealings of the irradiated crystals. The crystals irradiated at 10^{17} cm^{-2} have been annealed 30 min at 300 K while the crystals irradiated at 5×10^{17} cm^{-2} have been aged at 300 K several weeks. The crystals irradiated at 1.3×10^{18} cm^{-2} have been annealed 30 min at 425 K. This behavior suggests that the negative ions are very stable and anneal at higher temperature than 425 K. It is possible to check this idea by analyzing the curves $\tau=f(T)$ obtained after annealing at different temperatures and displayed in Figs. 3 and 4.

The analysis of the curves $\tau=f(T)$ in Figs. 3 and 4 has been performed in a similar way as for the curves $\tau=f(T)$ in Fig. 5. However, for some of the curves in Figs. 3 and 4, the values on the low- and high-temperature plateaus have been extrapolated. For these curves, fits have also been made where the positron binding energy was fixed at 38–41 meV, which is the value obtained from the curves in Fig. 5 (see Table II). From

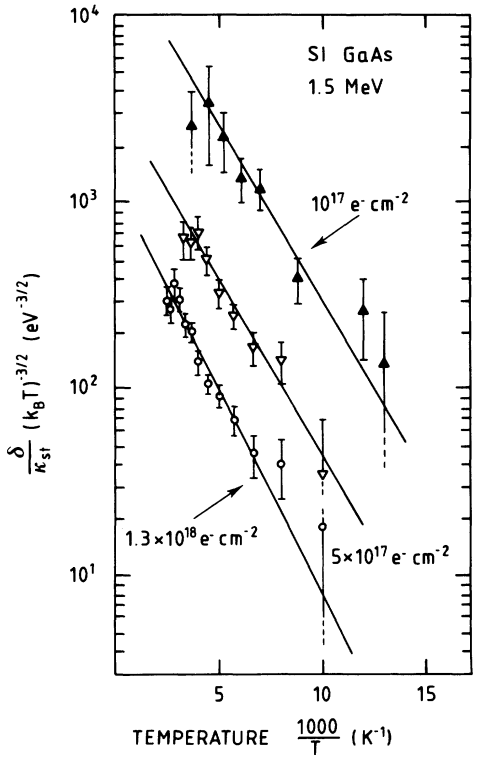

FIG. 7. Arrhenius plots for the positron detrapping rate δ from the Rydberg states around negative ions in semi-insulating GaAs after 1.5-MeV electron irradiation at 20 K. κ_{st} is the trapping rate at the ions. The fluences are 10^{17}, 5×10^{17}, and 1.3×10^{18} cm^{-2}. k_B is the Boltzmann constant and T the measurement temperature.

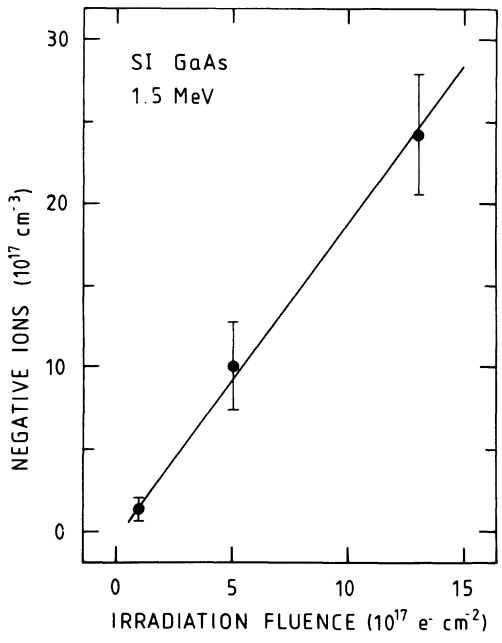

FIG. 8. Introduction rate of the negative ions as a function of fluence in semi-insulating GaAs after 1.5-MeV electron irradiation at 20 K. The aging temperature is 300 K for the fluences 5×10^{17} cm^{-2} and the annealing temperature is 300 K (30 min) for the fluences 10^{17} and 450 K (30 min) for the fluence 1.3×10^{17} cm^{-2}.

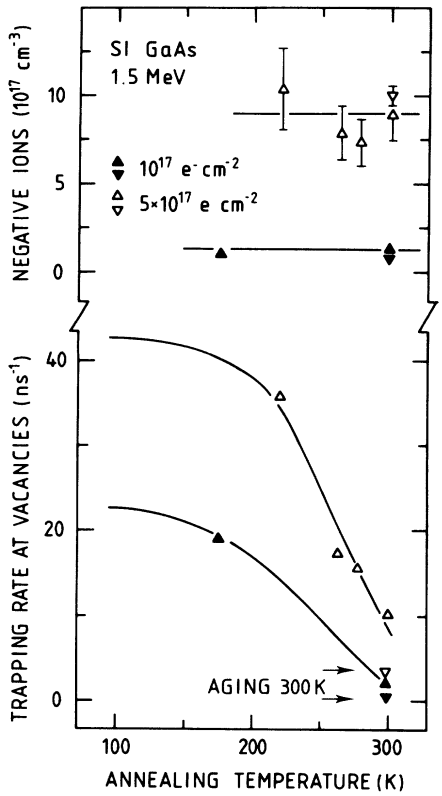

FIG. 9. Trapping rate at the vacancies κ_v and concentration of the ions c_{st} as functions of the annealing temperature in semi-insulating GaAs after 1.5-MeV electron irradiation at 20 K at the fluences 10^{17} and 5×10^{17} cm^{-2}.

this analysis, it is possible to obtain the trapping rates at vacancies and the concentrations of negative ions as function of the annealing temperatures. Figure 9 shows that the trapping rate at vacancies decreases strongly between 200–300 K indicating a strong vacancy recovery of about 70%. On the other hand, the concentration of negative ions remains constant in this temperature range, and it is also unaffected by the aging of the crystals at 300 K. This absence of recovery of the ions fits well with the proportionality of the ion production to the fluence in Fig. 8.

In summary, from our analysis of the positron-lifetime behavior, we found that electron irradiation produces monovacancies and negative ions in SI GaAs. The monovacancies start to recover below room temperature whereas the negative ions appear very stable with no recovery up to 425 K. The introduction rate of the negative ions is found to be high, 1.8 ± 0.3 cm^{-1} at 1.5-MeV electron irradiation.

VI. IDENTIFICATION OF THE VACANCIES AND NEGATIVE IONS

A. Gallium vacancies

In our earlier paper,[19] we have previously discussed the nature of the irradiation induced defects revealed by positrons using as main argument that the defects are negative in SI GaAs. We recall here the lines of our discussion and complete it.

It has been observed that positron trapping at native monovacancy defects disappear when the Fermi level decreases below $E_c-0.1$ eV (Ref. 15). We observe positron trapping at irradiation-induced monovacancy defects in irradiated SI GaAs when the Fermi-level position is at midgap. We can therefore conclude that the irradiation-induced monovacancy defects are different from the native monovacancy defects. The native monovacancy defects are neutral or positive in SI GaAs. The irradiation-induced monovacancy defects are neutral or negative in SI GaAs since they trap positive positrons.

The vacancies are able to compete at low temperatures with positron trapping at negative ions. This property provides good evidence that the monovacancies are negative rather than neutral. As we have earlier discussed,[2,15] arsenic vacancies are positive (V_{As}^{+}) in SI GaAs whereas gallium vacancies are negative (V_{Ga}^{3-}). Thus a simple explanation is that the gallium vacancy is involved in the irradiation-induced defects.

The annealing of the Ga vacancy starts at 80 K and occurs on a very broad temperature range up to 500 K (see Fig. 1). This broad stage is likely due to the large variety of defect configurations that irradiation can create (see Sec. V B). A sharp stage takes place between 270–370 K. No annealing is observed in the range 500–650 K at any measurement temperature although the lifetime is still above the bulk value. This means that the vacancy concentration remains constant in this temperature range. This is interesting as a major recovery stage detected by EPR measurements in SI GaAs and by DLTS measurements in n-type GaAs occurs between 500 and 650 K.[32] This recovery has been attributed to the recombination of different V_{As}-As_i pairs. The As vacancy is believed to be positively charged in SI GaAs, which is consistent with the absence of its detection by positrons. Small annealing stages have been observed previously by electrical measurements at about 235 K after electron irradiation[1] or at 180, 235, and 280 K after proton implantation in n-type GaAs.[33] Positron annihilation studies only have reported stages below 150 K in SI GaAs.[2,16,18] According to Würschum *et al.*[16] no vacancies are detected by positrons below 300 K when irradiation is performed at a low energy of 520 keV.

B. Gallium antisites

To discuss the nature of the irradiation-induced ions, we use the property that they are negative when the Fermi level is at about midgap. We assume that they are intrinsic defects, because we have observed them after irradiation in various crystals, n-type,[19] SI or even p-type.[34] Ion-type intrinsic defects that irradiation creates are interstitials (As_i or Ga_i) or antisites (As_{Ga} or Ga_{As}). The tetrahedral interstitials As_i, $(As_i)As_4$, or $(As_i)Ga_4$, and Ga_i, $(Ga_i)As_4$, or $(Ga_i)Ga_4$, are generally believed to be positive for any Fermi-level position in the gap.[21–25] As_{Ga} antisites are positive at midgap according EPR and electron-nuclear double resonance (ENDOR) experiments.[35,36] Only Ga_{As} antisites have been proposed to be negative at and below midgap. Two ionization levels ly-

ing below midgap at E_v+78 meV and E_v+203 meV above the maximum E_v of the valence band[37] have been identified in Ga-rich as-grown crystals[38–40] and after ion implantation.[41] They have been assigned by various authors to a double acceptor proposed to be the Ga antisites. If we believe that the charges previously attributed to ion-type intrinsic defects in GaAs are correct, we are lead to conclude that positrons after electron irradiation detect a large amount of Ga_{As} antisites.

Let us examine more carefully to which positron state the positron binding energy E_b governing the detrapping from the ions is related. According to recent calculations,[42] positrons once trapped at a Rydberg state can annihilate there or detrap back to the bulk but cannot make a transition to a deeper Rydberg state. In other words, a cascade capture process at successively deeper Rydberg states is not possible for positrons because of their short lifetime. The trapping coefficient from the bulk state to a Rydberg state decreases by about one order of magnitude as the quantum number n decreases by one unit.[42] The positron binding energy E_b determined from Fig. 7 corresponds to the lowest Rydberg state that the positron can reach. In the effective-mass theory,[43] we can calculate the ionization energy of the Rydberg state associated to a shallow acceptor and compare them to the positron binding energy E_b. Using a value of 12.9 for the dielectric constant ϵ and an effective mass of 1 for the positron in the relation

$$E_n=\frac{13.6\text{ eV}}{\epsilon^2}\left[\frac{m^*}{m}\right]\frac{Z^2}{n^2}\,, \tag{10}$$

we obtain the energy levels E_n for the acceptor charge $Z=1,2,3$ listed in Table IV.

In Table IV, the energy levels $n=3$ for $Z=2$ and $n=4$ for $Z=3$ have an energy of the same order as the positron binding energy of 41 ± 4 meV, but none of the levels for $Z=1$ have such a value. According to the ionization levels, the Ga_{As} antisite carries a double negative charge in SI GaAs. So it seems that the lowest state reached by the positron around the negative ion corresponds to $n=3$. The calculated ionization energy of the positron in the Rydberg state can be adjusted to the experimental value by increasing the positron effective mass to 1.1 ± 0.1 which is a reasonable value for GaAs.[24]

As we have seen above, positrons give evidence that irradiation induces negative vacancies and negative ions in SI GaAs. Therefore we reach the conclusion that acceptorlike defects exist after irradiation, when the Fermi level is around midgap. Electron irradiation has also been found to create acceptors in n-type GaAs after electrical measurements. From the Hall measurements performed in n-type GaAs, Look and Sizelove[3,4] have concluded that acceptorlike defects are created below $E_c-0.295$ eV in n-type GaAs by electron irradiation. Siyanbola and Palmer[33] have concluded from their reverse-bias capacitance-voltage measurements that proton irradiation creates acceptorlike levels lying in the lower half of the band gap in n-type GaAs. By confronting these results, we can conclude that a part of the irradiation-induced defects exhibits acceptor property both in n-type GaAs and in SI GaAs. This suggests that they have the same nature, ions, and/or vacancies from our measurements, in n-type GaAs and SI GaAs. In addition, the positrons results show and support the finding of Siyanbola and Palmer[33] that a part of the acceptors detected in n-type GaAs have their $1\longrightarrow0$ ionization levels below midgap, namely, the gallium antisites.

Look and Sizelove[3,4] determined that there is an introduction rate of 5 cm^{-1} for the acceptors in GaAs after room-temperature irradiation. We can use this value to calculate the introduction rate of the gallium vacancies $R(V_{Ga})$ when in addition we make the two following assumptions. The validity of these assumptions will not be discussed here, because, as we shall see, we use them as a necessary step to our purpose which is to make some estimation of the positron trapping coefficient at the gallium vacancies. First, we assume that the acceptors detected by Look and Sizelove are the Ga antisites and the Ga vacancies. This leads to

$$3R(V_{Ga}^{3-})+2R(Ga_{As}^{2-})=5\text{ cm}^{-1}\,. \tag{11}$$

Second, we assume that the introduction rate of the antisites is the same at 20 K and room temperature, i.e., 1.8 cm^{-1}. Equation (11) then gives that the introduction rate of the gallium vacancies is about 0.46 cm^{-1}. We make then the third assumption that the amount of gallium vacancies produced by room-temperature irradiation is about the same as the amount of gallium vacancies remaining after annealing at room temperature. This means that we consider that after aging at 300 K the total positron trapping rate at the vacancies κ_v is due to a concentration of vacancies c_v given by 0.46 cm^{-1} times the irradiation fluence. From the values κ_v given in Table III and the corresponding values c_v, we can then estimate from Eq. (3) that the positron trapping coefficient is $(3.1\pm0.5)\times10^{-8}$ cm^{-3} s^{-1} or, with $n_{atoms}=4.4\times10^{22}$ cm^{-3} in GaAs, $\mu_v=(1.4\pm0.2)\times10^{15}$ $atoms^{-1}$ s^{-1}.

The main result of our study is that irradiation produces a large amount of gallium antisites. It is the first time that a high value for the production rate of Ga_{As} is reported. It has been earlier suggested from one-phonon absorption data[44] that gallium antisites were produced by neutron irradiation in n-type and SI GaAs. The infrared resonant mode associated with the gallium antisites showed a maximum annealing at a temperature depending on the fluence. The temperature decreased from 400 °C to 320 °C as the fluence increased by an order of magnitude from 1.3×10^{18} to 18×10^{18} cm^{-2}. In our case, there is no need to reach such high temperatures to

TABLE IV. Ionization energies in meV of the Rydberg states n in the effective-mass theory. Z is the ion charge. The dielectric constant is taken equal to 12.9 and the positron effective mass to 1.0.

Charge	$n=1$	$n=2$	$n=3$	$n=4$	$n=5$	$n=6$
$Z=1$	82	20	9	5	3.3	2.2
$Z=2$	328	80	36	20	13	8.8
$Z=3$	738	180	81	46	29.5	20.5

observe the gallium antisites. Contrary to the case of the gallium antisite, it has been shown by EPR measurements that the arsenic antisites (for a review see Refs. 6 and 12) are produced after electron[8,9] and neutron irradiation.[10,11] The concentration of antisites after neutron irradiation increases with fluence in SI GaAs (Ref. 11). After electron irradiation in n-type or SI GaAs, the fluence dependence is more complicated[8,9,45] and more data would be valuable. The formation of As antisites seems to show a saturation level depending on the doping concentration.[8,9,45]

The literature concerning the mechanisms of defect formation by electron irradiation in GaAs (for a review see Ref. 13) and, more generally in compound semiconductors, is rather rare. After electron irradiation, a great variety of defects and defect complexes can be formed by direct collision and collision replacement mechanisms. Reflecting this variety, the EPR quadruplet spectra usually modeled by an isolated As antisite $(As_{Ga})As_4$ may be more carefully analyzed according to Ref. 6 and then show broad components likely due to $(As_{Ga})As_{4-n}X_n$ complexes. However, it remains that there is evidence from the EPR data and from our positron data that irradiation produces the isolated antisites of both types. The linear dependence with fluence we found for the Ga_{As} antisites suggests that they are primary defects or formed by the immediate rearrangement of a primary defect.

VII. CONCLUSION

In this work, positron-lifetime measurements performed after 1.5-MeV electron irradiation show very clearly that acceptors are created in SI GaAs by electron irradiation. Two types of acceptors can be separated. The first ones are vacancy type and anneal over a very broad range of temperature between 77 K and 500 K. The second ones are ion-type and anneal at high temperature above 450 K. The data show that these two types of defects are independent and do not form close pairs. We attribute both to gallium-related defects. The negative ion-type defects exhibit the properties expected from isolated gallium antisites, and they are consequently identified to isolated gallium antisites. The negative vacancy-type defects are identified with gallium vacancies which are isolated or involved in negatively charged complexes.

The introduction rate of the gallium antisite is determined to be 1.8 ± 0.3 cm^{-1} in the fluence range of $(1-13)\times10^{17}$ cm^{-2} when 1.5-MeV electron irradiation is performed at 20 K with subsequent annealing at 77 K.

Positrons do not detect any annealing stage for the vacancy-type defects in the temperature range 500–650 K where other techniques like EPR or electrical measurements give evidence of strong recovery. This recovery is associated to the arsenic vacancy which disappears in this annealing stage by recombination with As_i interstitials. The absence of this stage in positron measurements is consistent with the positive charge state of the arsenic vacancy.

The positron data analyzed in this work for SI GaAs and electrical data previously analyzed for n-type GaAs (Refs. 3, 4, and 33) lead to the same conclusion that acceptors with their ionization levels below midgap are produced by electron irradiation. From the positron data in SI GaAs, it can be inferred that the gallium vacancy V_{Ga}^{3-} and the gallium antisite Ga_{As}^{2-} are responsible for a part of the acceptors lying below midgap in n-type GaAs. The assumption that they represent the total concentration of acceptors leads to an introduction rate of the gallium vacancies of about 0.5 cm^{-1} at room-temperature irradiation when the total acceptors introduction rate of is taken to be 5 cm^{-1} from the data of Look and Sizelove.[3,4]

APPENDIX

In this appendix we shall discuss in more detail the three-state positron trapping model used to analyze our experimental data. In addition to delocalized state in the bulk, the positron in our model can get trapped at vacancy defects or at negative ions. The detrapping back to the bulk state is possible from the negative ions ("shallow" traps) but not from the vacancy defects ("deep" traps). Using model calculations, we shall discuss successively the influence of positron trapping and detrapping rates, and the positron binding energy at negative ions to the temperature dependence of our measurement parameter, the average positron lifetime.

The kinetic equations describing transitions between bulk, vacancy, and ion states are the following:

$$\begin{aligned}
\frac{dn_b}{dt} &= -\lambda_b n_b - \kappa_v n_b - \kappa_{st} n_b + \delta n_{st} , \\
\frac{dn_{st}}{dt} &= -\lambda_{st} n_{st} - \delta n_{st} + \kappa_{st} n_b , \\
\frac{dn_v}{dt} &= -\lambda_v n_v + \kappa_v n_b ,
\end{aligned} \tag{A1}$$

where $n_b(t)$, $n_v(t)$, and $n_{st}(t)$ are the number of positrons at the bulk, vacancy, and ion states, respectively. As an initial condition at $t=0$, all positrons n_0 are assumed to be thermalized at the delocalized state $[n_b(0)=n_0$, $n_v(0)=0$, and $n_{st}(0)=0]$. λ_i, κ_i, and δ_i indicate the annihilation, trapping, and detrapping rates from the state i, respectively.

From the general solution $n(t)=n_b(t)+n_{st}(t)+n_v(t)$ of the differential equations (A1) (see, e.g., Ref. 46), the average positron lifetime can be calculated as

$$\tau = \frac{\int_0^\infty t \left[-\frac{dn}{dt} \right] dt}{\int_0^\infty \left[-\frac{dn}{dt} \right] dt} . \tag{A2}$$

The evaluation of the integrals in Eq. (A2) yields to Eq. (5), which is used in the analysis of the experimental data in Sec. V. Notice that Eq. (5) is obtained also directly by solving Eqs. (A1) for the stationary state ($dn_i/dt=0$).

The ratio δ/κ_{st} in Eq. (5) can be expressed in terms of the positron binding energy E_b and the negative ion concentration c_{st} using Eq. (6) to describe the populations of

the delocalized and the trapped positron states at temperature T (Sec. V). To get information on the parameters E_b and c_{st}, Eqs. (5) and (6) can thus be fitted to the experimental values of the average positron lifetime. In the following, we shall investigate qualitatively the influences of E_b and c_{st} as well as the trapping and detrapping rates κ_v, κ_{st} and δ to the shape of the average lifetime as a function of temperature T. In our model calculations, we use the parameter values corresponding to electron irradiated semi-insulating GaAs with $\tau_v=\lambda_v^{-1}=260$ ps and $\tau_b=\lambda_b^{-1}=\tau_{st}=\lambda_{st}^{-1}=230$ ps. The trapping rates κ_v and κ_{st} were kept independent of temperature, and they were related to each other by Eq. (8) (see Sec. V) in the low-temperature limit, where the detrapping is negligible ($\delta=0$). The effective mass $m^*=m$ was used.

Let us first increase the trapping rate κ_v at vacancies from 0.02 κ_{st} to 200 κ_{st}, and let the other parameters be constant ($\kappa_{st}=22.3$ ns^{-1}, $c_{st}=10^{18}$ cm^{-3}, $E_b=50$ meV). The detrapping rate $\delta=f(T)$ remains thus the same while κ_v varies. The average lifetime from Eq. (5) is shown for these parameters in Fig. 10. For a too small ratio κ_v/κ_{st}, there is no effect from the vacancies, and the average lifetime remains 230 ps at all temperatures. When the ratio κ_v/κ_{st} increases, the lifetime increases and the low- and high-temperature plateaus start to appear. The temperatures at which these plateaus exist remain nearly unchanged for κ_v/κ_{st} in the range of 0.05–5. When κ_v/κ_{st} increases further, the beginning of the high-temperature plateau tends to shift to lower temperatures. Finally, the effect of negative ions is lost, and the lifetime remains saturated at the value of 260 ps at all temperatures. The evolution of the curves $\tau=f(T)$ in the range $\kappa_v/\kappa_{st}=0.05-1$ reproduces well the experimentally observed behavior in Figs. 3 and 4, when aging at 300 K reduces the trapping rate at vacancies.

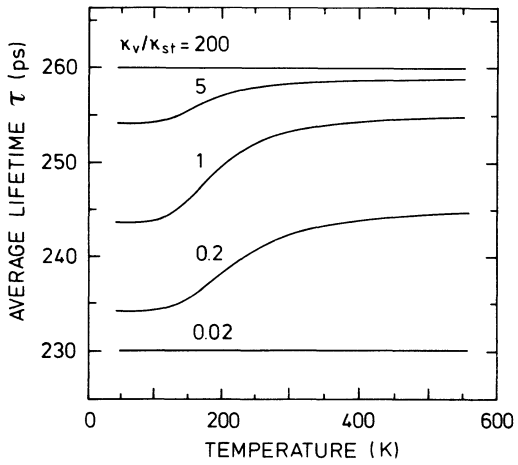

FIG. 10. Temperature dependence of the average lifetime in the presence of vacancies and shallow traps (negative ions) as calculated from Eq. (5). The ratio of the trapping rate at the vacancies κ_v to the trapping rate at the negative ions κ_{st} varies. The fixed parameters in the calculations are $\kappa_{st}=22.3$ ns^{-1}, the ion concentration $c_{st}=10^{18}$ cm^{-3}, and the positron binding energy at the ions $E_b=50$ meV.

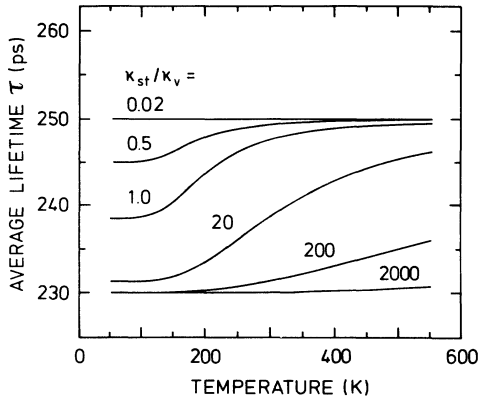

FIG. 11. Temperature dependence of the average lifetime as a function of the trapping rate at the negative ions κ_{st} as calculated from Eq. (5). The ratios of the trapping rate at the negative ions κ_{st} to the trapping rate at the vacancies kv is indicated for each curve. The trapping coefficient at the negative ions $\mu_{st}=\kappa_{st}/c_{st}$ is fixed to 10^{15} cm^{-2} and κ_{st} varies via the ion concentration. The parameters fixed in the calculation of the average lifetime are $\kappa_v=8.7$ ns^{-1} for the trapping rate at the vacancies and $E_b=50$ meV for the positron binding energy at the ions, respectively.

Figure 11 shows the effect of an increase in the positron trapping rate at the negative ions κ_{st} in the range of $\kappa_{st}=0.20\kappa_v-2000\kappa_v$. The positron trapping coefficient at the negative ions $\mu_{st}=f(T)$ is fixed at $\mu_{st}=10^{15}$ s^{-1}, and the concentration of negative ions thus increases by five orders of magnitude. The trapping rate at vacancies and the positron binding energy at negative ions are constant at values of $\kappa_v=8.7$ ns^{-1} and $E_b=50$ meV, respectively.

When the ratio κ_{st}/κ_v is small ($\kappa_{st}/\kappa_v<0.1$), there is no effect of the negative ions, and the lifetime is constant

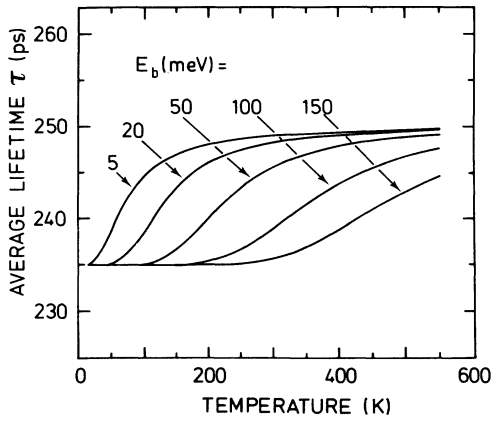

FIG. 12. Temperature dependence of the average lifetime as a function of the positron binding energy at the ions as calculated from Eq. (5). The ratios of the trapping rate at the vacancies κ_v to the trapping rate at the negative ions κ_{st} is 0.22. The parameters fixed in the calculation of the average lifetime have the value $\kappa_v=8.7$ ns^{-1} for the trapping rate at the vacancies, $\kappa_{st}=39.1$ ns^{-1} for the trapping rate at the ions and 1.7×10^{18} cm^{-3} for the ion concentration.

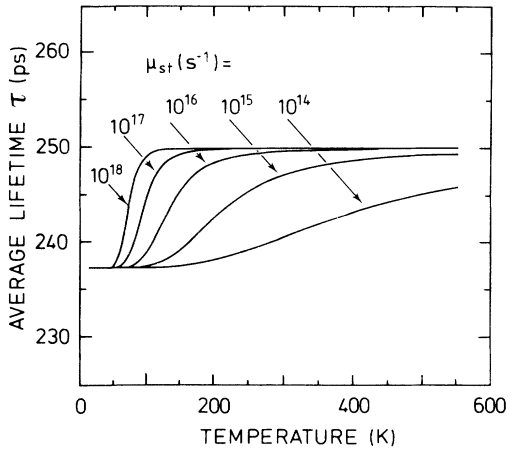

FIG. 13. Temperature dependence of the average lifetime as a function of the positron trapping coefficient μ_{st} as calculated from Eq. (5). The ratio of the trapping rate at the vacancies κ_v to the trapping rate at the negative ions is $\kappa_{st}=0.39$. The parameters fixed in the calculation of the average lifetime have the values $\kappa_v=8.7$ ns^{-1} for the trapping rate at the vacancies and $\kappa_{st}=22.3$ ns^{-1} for the trapping rate at the ions. The trapping coefficient at the ions is indicated for each curve. The ion concentration increases by four orders of magnitude as the trapping coefficient at the ions decreases by four orders of magnitude.

at all temperatures. When the ratio κ_{st}/κ_v increases, the plateau at low temperature begins to appear, and the curve $\tau=f(T)$ increases from this plateau to the plateau at high temperatures. As κ_{st}/κ_v increases further, the curves are deformed as follows. The onset of the plateau at high temperatures increases strongly, and temperatures higher than 700 K must be reached to see a temperature-independent average lifetime for $\kappa_{st}/\kappa_v=20$. However, the range of a constant lifetime at low temperatures is nearly unaffected. The value of the lifetime on the plateau at low temperatures decreases, but the lifetime value on the high-temperature plateau remains unchanged. The shape of the curves in Fig. 11 reproduces well the experimentally observed behavior in Fig. 5. Hence, the evolution of the curves in Fig. 5 corresponds to an increase in the positron trapping rate κ_{st}, when the irradiation fluence increases.

In Fig. 12, the influence of the positron binding energy E_b at the negative ions is shown in the range from 5 to 150 meV. The other parameters are fixed at values of $\kappa_v=8.7$ ns^{-1}, $\kappa_{st}=39.1$ ns^{-1}, and $c_{st}=1.7\times10^{18}$ cm^{-3}. For a given temperature, the detrapping rate $\delta=f(T)$ thus decreases as E_b increases. As the ratio κ_v/κ_{st} is constant, the lifetime values on the plateaus at high and low temperatures remain unchanged. The onset temperatures for the end of the low-temperature plateau and for the beginning of the constant high-temperature region are seen to depend directly on E_b. For example, when the binding energy increases from 20 to 50 meV, there is a shift of about 50 and 100 K for the low- and high-temperature plateaus, respectively. The width of the transition between the two regions of constant $\tau=f(T)$ increases strongly with E_b: it is about 200 K for 25 meV and it increases up to about 400 K for 100 meV.

Figure 13 shows the changes in the average lifetime curves, when the positron trapping coefficient $\mu_{st}=\kappa_{st}/c_{st}$ at negative ions is varied from 10^{14} to 10^{18} s^{-1}. The calculations have been done with $\kappa_v=8.7$ ns^{-1}, $\kappa_{st}=22.3$ ns^{-1}, and $E_b=50$ meV. When the trapping coefficient μ_{st} becomes smaller, the detrapping rate $\delta=f(T)$ decreases. Then, the detrapping from the negative ions becomes more difficult, and the effects of the vacancies less visible. The deformation of the shape of the curves is the following as the trapping coefficient μ_{st} decreases. The lifetimes on the high- and low-temperature plateaus remain constant. The low-temperature plateau ends roughly at the same temperature (about 100 K for $E_b=50$ meV), but the slopes in the $\tau=f(T)$ curve become smaller. The beginning of the high-temperature plateau is shifted to higher temperatures, when the trapping coefficient μ_{st} decreases. The shape of the experimental curves in Figs. 3–5 is reproduced, when μ_{st} is between 10^{15} and 10^{16} s^{-1}.

[1]A. A. Rezazadeh and D. W. Palmer, J. Phys. C **18**, 43 (1985).
[2]P. Hautojärvi, P. Moser, M. Stucky, C. Corbel, and F. Plazaola, Appl. Phys. Lett. **48**, 809 (1986).
[3]D. C. Look and J. R. Sizelove, J. Appl. Phys. **62**, 3660 (1987).
[4]D. C. Look, Solid State Commun. **64**, 805 (1987).
[5]H. J. von Bardeleben and J. C. Bourgoin, Phys. Rev. B **33**, 2890 (1986).
[6]A. Goltzené and C. Schwab, Phys. Status Solidi B **160**, 649 (1990).
[7]R. Wagner, J. Krebs, G. Stauss, and A. White, Solid State Commun. **36**, 15 (1980).
[8]N. Goswani, R. Neuwman, and J. Whitehouse, Solid State Commun. **40**, 473 (1981).
[9]H. J. von Bardeleben and J. C. Bourgoin, J. Appl. Phys. **58**, 1041 (1985).
[10]R. Wirner, U. Kaufmann, and J. Schneider, Appl Phys. Lett. **40**, 141 (1982).
[11]A. Goltzené and C. Schwab, Appl. Phys. Lett. **54**, 907 (1989).
[12]J. C. Bourgoin, H. J. von Bardeleben, and D. Stievenard, J. Appl. Phys. **64**, 65 (1988).
[13]D. Stievenard, J. C. Bourgoin, and D. Pons, Physica B+C **116B**, 394 (1983); D. Pons and J. C. Bourgoin, J. Phys. C **18**, 3839 (1985).
[14]G. Dlubek, R. Krause, O. Brümmer, and J. Tittes, Appl. Phys. A **42**, 125 (1987).
[15]C. Corbel, M. Stucky, P. Hautojärvi, K. Saarinen, and P. Moser, Phys. Rev. B **38**, 8192 (1988).
[16]R. Würschum, W. Bauer, K. Maier, A. Seeger, and H. E. Schaefer, J. Phys. Condens. Matter **1**, SA33 (1989).
[17]J. Mäkinen, C. Corbel, P. Hautojärvi, P. Moser, and F. Pierre, Phys. Rev. B **39**, 10 162 (1989).
[18]R. Würschum and H. E. Schaefer, Phys. Status Solidi A **103**, 101 (1987).
[19]C. Corbel, F. Pierre, P. Hautojärvi, K. Saarinen, and P. Moser, Phys. Rev. B **41**, 10 632 (1990).
[20]P. Mascher, D. Kerr, and S. Dannefaer, J. Cryst. Growth **85**, 295 (1987); Cryst. Res. Technol. **23**, 247 (1988).
[21]J. van der Rest and P. Pécheur, J. Phys. C **17**, 85 (1984).

[22]G. A. Baraff and M. Schlüter, Phys. Rev. Lett. **55**, 2340 (1985).
[23]S. Loualiche, A. Nouailhat, G. Guillot, and M. Lannoo, Phys. Rev. B **20**, 5822 (1984).
[24]M. J. Puska, J. Phys. Condens. Matter **1**, 7347 (1989).
[25]Hongqi Xu and U. Lindefelt, Phys. Rev. B **41**, 5979 (1990).
[26]*Positrons in Solids,* edited by P. Hautojärvi, Topics in Current Physics Vol. 12 (Springer, Heidelberg, 1979).
[27]*Positron Solid State Physics,* edited by W. Brandt and A. Dupasquier (North-Holland, Amsterdam, 1983).
[28]M. Puska, O. Jepsen, O. Gunnarsson, and R. Nieminen, Phys. Rev. B **34**, 2695 (1986); M. J. Puska, Phys. Status Solidi A **102**, 11 (1987).
[29]M. J. Puska and C. Corbel, Phys. Rev. B **38**, 9874 (1988).
[30]K. Saarinen, P. Hautojärvi, A. Vehanen, R. Krause, and G. Dlubek, Phys. Rev. B **39**, 5287 (1989).
[31]M. Manninen and R. Nieminen, Appl. Phys. A **26**, 93 (1981).
[32]D. Stievenard, X. Boddaert, J. Bourgoin, and H. J. von Bardeleben, Phys. Rev. B **41**, 5271 (1990).
[33]W. O. Siyanbola and D. W. Palmer, Phys. Rev. Lett. **66**, 56 (1991).
[34]F. Pierre, Ph.D. thesis (unpublished).
[35]H. J. von Bardeleben, J. C. Bourgoin, and A. Miret, Phys. Rev. B **34**, 1360 (1986).
[36]H. J. von Bardeleben and D. Stievenard, in *Defects in Electronic Materials,* edited by M. Stavola, S. J. Pearton, and G. Davies (Materials Research Society, Pittsburgh, 1987), p. 351.
[37]G. Roos, A. Schoner, G. Pensi, K. Krambrock, B. K. Meyer, J. M. Spaeth, and J. Wagner, in *Defects in Semiconductors,* edited by G. Ferenczi, Materials Science Forum (Trans Tech, Aedermannsdorf, Switzerland, 1989), Vols. 38–41, p. 951.
[38]W. C. Mitchell, G. J. Brown, D. W. Fischer, P. W. Yu, and J. E. Lang, J. Appl. Phys. **62**, 2320 (1987).
[39]M. Bugajski, K. H. Ko, J. Lagowski, and H. C. Gatos, J. Appl. Phys. **65**, 596 (1989).
[40]J. Wagner, Phys. Scr. T **29**, 167 (1989).
[41]M. Dansas, J. Appl. Phys. **55**, 3617 (1979).
[42]M. Puska, C. Corbel, and R. Nieminen, Phys. Rev. B **41**, 9980 (1990).
[43]G. Burns, *Solid State Physics* (Academic, London, 1985).
[44]J. D. Collins, G. A. Gledhill, and R. C. Newmann, in *Defects in Semiconductors,* edited by J. H. von Bardeleben, Materials Science Forum (Trans Tech, Aedermannsdorf, Switzerland, 1986), Vols. 10–12, p. 265.
[45]A. Goltzené, B. Meyer, C. Schwab, R. B. Beall, R. C. Newmann, J. E. Whitehouse, and J. Woodhead, J. Appl. Phys. **57**, 5196 (1985).
[46]B. Pagh, H. E. Hansen, B. Nielsen, G. Trumpy, and K. Petersen, Appl. Phys. **33**, 255 (1984).